Electronic Supplementary Material (ESI) for Metallomics.

SUPPLEMENTARY INFORMATION

High affinity interactions of Pb^{2+} with Synaptotagmin I

Sachin Katti,[1] Bin Her, [1] Atul K. Srivastava,[1] Alexander B. Taylor,[2] Steve W. Lockless,[3] and Tatyana I. Igumenova[1,*]

[1]Department of Biochemistry and Biophysics, Texas A&M University, 300 Olsen Boulevard, College Station, TX 77843, United States

[2]Department of Biochemistry and Structural Biology and the X-ray Crystallography Core Laboratory, Institutional Research Cores, University of Texas Health Science Center at San Antonio, San Antonio, TX 78229, United States

[3]Department of Biology, Texas A&M University, 3258 TAMU, TX 77843, United States

METHODS

Expression and purification of SytI C2 domains

Genes expressing the following SytI domains: C2A (residues 137-265), C2B (residues 271-421), and C2AB (residues 137-421) were cloned into pET-SUMO vector (Novagen, Madison, WI) and expressed as SUMO fusion proteins to improve the solubility and yield. In addition, the QuikChange mutagenesis kit (Stratagene, La Jolla, CA) was used to: (i) introduce a Serine residue at the N-terminus of C2A-containing constructs which improved the SUMO cleavage efficiency, and (ii) replace a sole Cysteine on C2B at position 277 with a Serine to avoid the use of reducing agents that can potentially interact with divalent metal ions.

All chromatography columns were acquired from GE Healthcare. SytI domains fused to 6xHis-tagged SUMO were expressed in BL21(DE3) (C2A and C2AB) and Rosetta(DE3) (C2B) cells and partially purified on HisTrap HP columns, followed by the removal of 6xHis-SUMO (using SUMO protease), as previously described.[1] To prepare [U-^{15}N] enriched proteins, the cells were resuspended in M9 medium containing [U-^{15}N] NH_4Cl (Cambridge Isotope Laboratories) during protein expression. The final purification step involved an anion (cation)-exchange chromatography on the HiTrap Q (HiTrap SP) HP column for the C2A and C2AB (C2B). 100 μM EDTA was used in all ion-exchange chromatography buffers to ensure that the purified protein remains free of any divalent metal ions. Prior to use, the concentrated protein stocks were subjected to four successive passes through the desalting PD MidiTrap G-25 columns to achieve exchange into experiment-specific buffers and removal of residual EDTA.

Crystal structure determination and refinement

The C2 crystals were transferred to undersized cryo-loops and excess mother liquor was removed prior to flash-cooling in liquid nitrogen. X-ray diffraction data were acquired using a home source Rigaku MicroMax 007HF X-ray Generator equipped with VariMax HR and HF confocal optics and RAXIS-HTC image plate detectors. Integration and scaling of the diffraction data was done using XDS.[2] The C2A structure was determined with the molecular replacement method implemented in PHASER[3] using the Protein Data Bank entry 3F00 as a search model. The initial search model coordinates contained some additional amino-terminal residues that were absent from the C2A construct used in this study. Therefore, a compact search model that passed packing function analysis was created by truncating the extended

amino-terminus and some loop regions to yield successful molecular replacement solutions. Similarly, the C2B structures were determined by the molecular replacement method using coordinates from Protein Data Bank entry 1uow[4] as a search model. Coordinates were refined using PHENIX[5], including simulated annealing with torsion angle dynamics, and alternated with manual rebuilding using COOT.[6] Note on the identification of heavy metal ion sites: the difference Fourier maps of each structure mentioned above were used to verify that the modeled Pb^{2+} are indeed heavy atoms (compared to the anomalous signal observed for sulfur atoms in the proteins). Anomalous peaks are observed at 81.3 and 69.4 r.m.s.d. for the two C2A proteins in the C2A-Pb^{2+} asymmetric unit. Anomalous peaks are observed at 27.5 r.m.s.d. for low-occupancy C2B-Pb^{2+} and 24.4 r.m.s.d. for high-occupancy C2B-Pb^{2+}.

Analysis of the ZZ exchange NMR data

The analysis of the intensity data was carried out as described by Miloushev et al.[7] Residue-specific composite peak intensity ratios, Ξ, were calculated using the following equation:

$$\Xi = \frac{I_{ab} \cdot I_{ba}}{I_a \cdot I_b - I_{ab} \cdot I_{ba}} = k_{on}^{'} k_{off} \cdot t_{mix}^2 \qquad \text{(S1)}$$

where I_{ab} and I_{ba} are the cross-peak, and I_a and I_b are the auto-peak intensities, respectively; t_{mix} is the mixing time; and k_{on}' and k_{off} are the Pb^{2+} association and dissociation rate constants in the following reaction scheme:

$$C2 + Pb^{2+} \underset{koff}{\overset{kon'}{\rightleftharpoons}} C2.Pb^{2+} \qquad \text{(S2)}$$

k_{on}' is defined as:

$$k_{on}^{'} = k_{on} \cdot [\,Pb^{2+}\,]_{free} \qquad \text{(S3)}$$

The product of k_{on}'·k_{off}, ζ, was obtained by globally fitting the experimental data Ξ(t_{mix}) using **Eq. S1** (**Fig. S4a**). The ratio of the two rate constants, k_{off} /k_{on}', is given by the apparent dissociation constant $K_{d,app}$ of the binding reaction. To determine $K_{d,app}$, we acquired the fully relaxed (recycle delay of 6 s) ^{15}N-^{1}H HSQC spectra at all 4 temperatures for both domains. The residue-specific $K_{d,app}$ values were calculated as the ratio of the auto- and cross-peak volumes:

$$K_{d,app} = \frac{V_a + V_{ab}}{V_b + V_{ba}} = \frac{k_{off}}{k_{on}^{'}} \qquad \text{(S4)}$$

and then averaged to get the final $K_{d,app}$ values plotted in **Fig. S4b**. Individual rate constants k_{on}' and k_{off} were obtained from their product ζ (**Eq. 3**) and $K_{d,app}$ (**Eq. 6**). The association rate constant k_{on} was calculated using the following equations:

$$\frac{K_d}{K_{d,app}} = \frac{k_{off}/k_{on}}{k_{off}/k_{on}'} = \frac{k_{on}'}{k_{on}} \quad \text{(S5)}$$

$$\therefore k_{on} = k_{on}' \frac{K_{d,app}}{K_d} \quad \text{(S6)}$$

where K_d is the dissociation constant. The K_d value was determined at 25 °C with ITC, and extrapolated to other temperatures using ΔH and ΔS values, assuming both are constant over the limited temperature range sampled. The kinetic parameters obtained with this analysis are given in **Table S6**.

To determine the activation enthalpy $\Delta H^{\neq}$ and entropy $\Delta S^{\neq}$ from the temperature dependent variations in k_{on} and k_{off}, we used the linear form of the Eyring equation:

$$ln\left(\frac{k}{T}\right) = -\frac{\Delta H^{\neq}}{R}\left(\frac{1}{T}\right) + ln\left(\frac{k_B}{h}\right) + \frac{\Delta S^{\neq}}{R} \quad \text{(S7)}$$

where T is temperature, k_B is the Boltzmann constant, h is the Planck constant, and R is the gas constant. The fits to **Eq. S7** are shown in **Fig. 5e** along with the relevant transition state parameters.

Tb^{3+} luminescence experiments

Purified recombinant C2AB was buffer-exchanged into a decalcified solution of 10 mM MES at pH 6.0 and 100 mM KCl. The emitted Tb^{3+} luminescence as a result of Trp to Tb^{3+} FRET was measured on a PC1 photon counting spectrofluorometer (ISS, Champaign, IL) at 25 °C with an excitation wavelength of 280 nm, and 1(2) nm slit widths on the excitation (emission) channels. In addition, a 370 nm cut-on filter was used on the emission channel to minimize the Trp emission and water Raman peak.

For the Tb^{3+} binding experiment, the aliquots of Tb^{3+} stock solution (buffer) were added to the sample (reference) cuvettes containing 2 ml of 2.5 μM C2AB domain. The sample dilution at the end of the experiments was maintained below 10%. The intensity of Tb^{3+} luminescence was monitored at the maxima of its most intense emission peak, 545 nm, with averaging over 60 measurements. The raw intensities from the reference were then subtracted from those of the

sample and corrected for dilution. To obtain the apparent binding affinity of Tb^{3+} to the C2AB domain, the data were fitted with the following equation:

$$I=(I_{max}/2P_0)[(K_d+P_0+L_0)-((K_d+P_0+L_0)^2-4P_0L_0)^{1/2}] \quad \text{(S8)}$$

where I is the intensity of Tb^{3+} luminescence at 545 nm; I_{max} is the intensity reached upon full C2AB saturation; and P_0 and L_0 are the total C2AB and Tb^{3+} concentrations, respectively. For the metal ion displacement experiments, Tb^{3+}-bound C2AB prepared by adding 20 μM Tb^{3+} to 2.5 μM protein. The Tb^{3+} luminescence intensity at 545 nm was monitored as a function of increasing $[M^{2+}]$, where M=Ca, Pb.

Vesicle co-sedimentation

Vesicle co-sedimentation assays were carried out with 5 μM C2A/C2B/C2AB as previously described,[1] in a buffer composed of 10 mM MES (pH 6.0) and 100 mM KCl. The protein was incubated at room temperature for 30 min with sucrose-loaded LUVs (100 nm-diameter, 1.5 mM total lipids with POPC:POPS=80:20), followed by 1 hr of further incubation after the addition of M^{2+} (M=Ca,Pb) to a final concentration of 0.1/0.2 mM. Control samples contained all components except the divalent metal ions and were treated in an identical manner. After incubation, the LUVs were pelleted using a tabletop ultracentrifuge (Optima™ MAX-XP, Beckman Coulter) for 30 min at 150,000 g and 25 ºC. The amount of unbound protein left in the supernatant was determined by Bicinchoninic acid (BCA) assay (Thermo Scientific) with BSA dilutions as standards. The fraction of protein bound to the vesicles, f_{bound}, was calculated as:

$$f_{bound}=\frac{P_0-P}{P_0} \quad \text{(S9)}$$

where P_0 is the total amount of protein in the sample and P is the amount of protein that remained in the supernatant after pelleting. Each sample was measured with BCA assay in duplicates. The results are shown in **Fig. S2.**

FIGURES

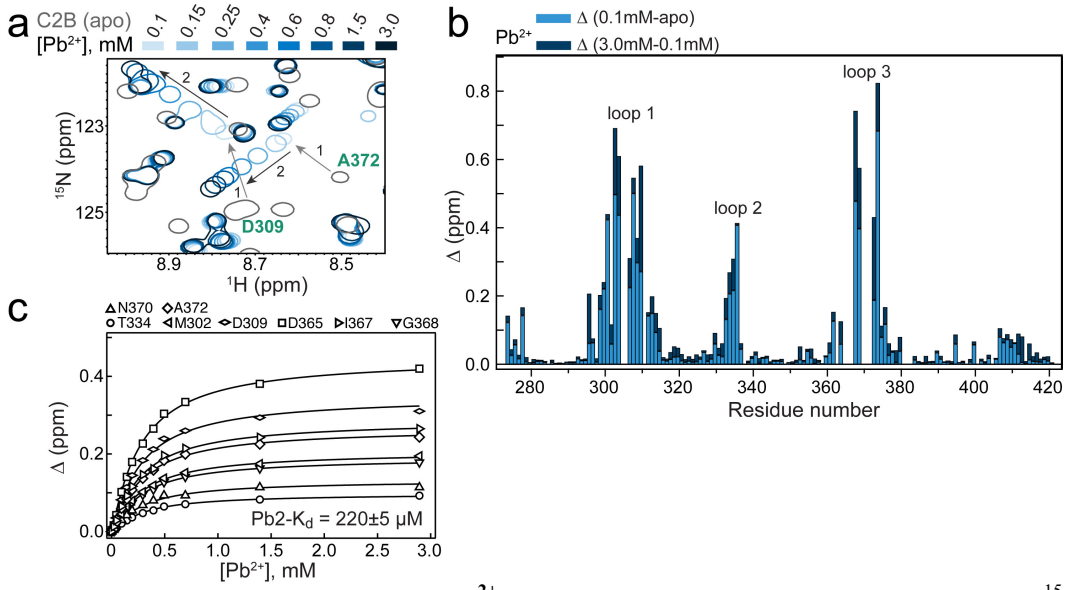

Figure S1. C2B domain binds two Pb^{2+} ions in solution. (**a**) Expansions of the C2B ^{15}N-^{1}H HSQC region for Pb^{2+} concentrations ranging from 0 to 3.0 mM. Peak displacements due to binding Pb1 (1, slow exchange) and Pb2 (2, fast exchange) are shown with arrows. (**b**) C2B chemical shift perturbation plot constructed for the low- (< 0.1 mM) and high- (> 0.1 mM) concentration regimes of Pb^{2+}. (**c**) NMR-detected binding curves constructed for the low-affinity Pb^{2+} site. Solid lines represent the global fit that produced the K_d of 220 ± 5 μM.

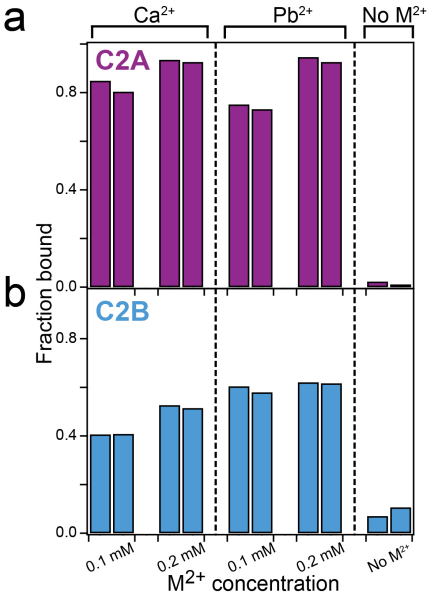

Figure S2. Pb^{2+} supports the membrane association of C2A and C2B domains. The fraction of membrane-bound C2A (**a**, purple) and C2B (**b**, blue) is plotted against M^{2+} concentration. The co-sedimentation experiments were carried out with phospholipid vesicles containing 20% (molar) phosphatidylserine component. The two adjacent bars at a given M^{2+} concentration represent two independent experiments.

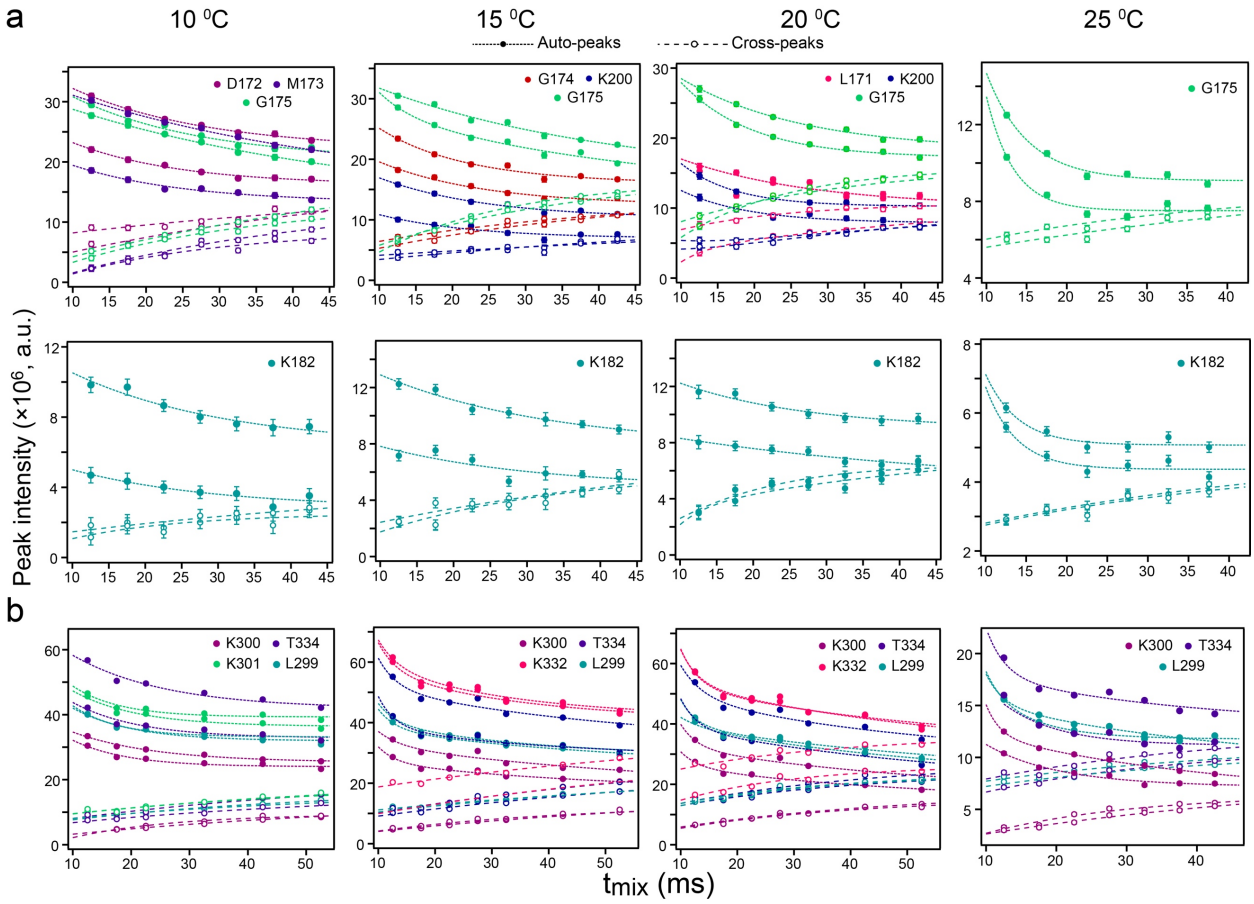

Figure S3. The dependence of auto- and cross-peak intensities on the mixing time, t_{mix}, in ZZ-exchange NMR experiments. The data are shown for the C2A (**a**) and C2B (**b**) domains at 4 different temperature values. Lines drawn through the experimental points are to guide the eye.

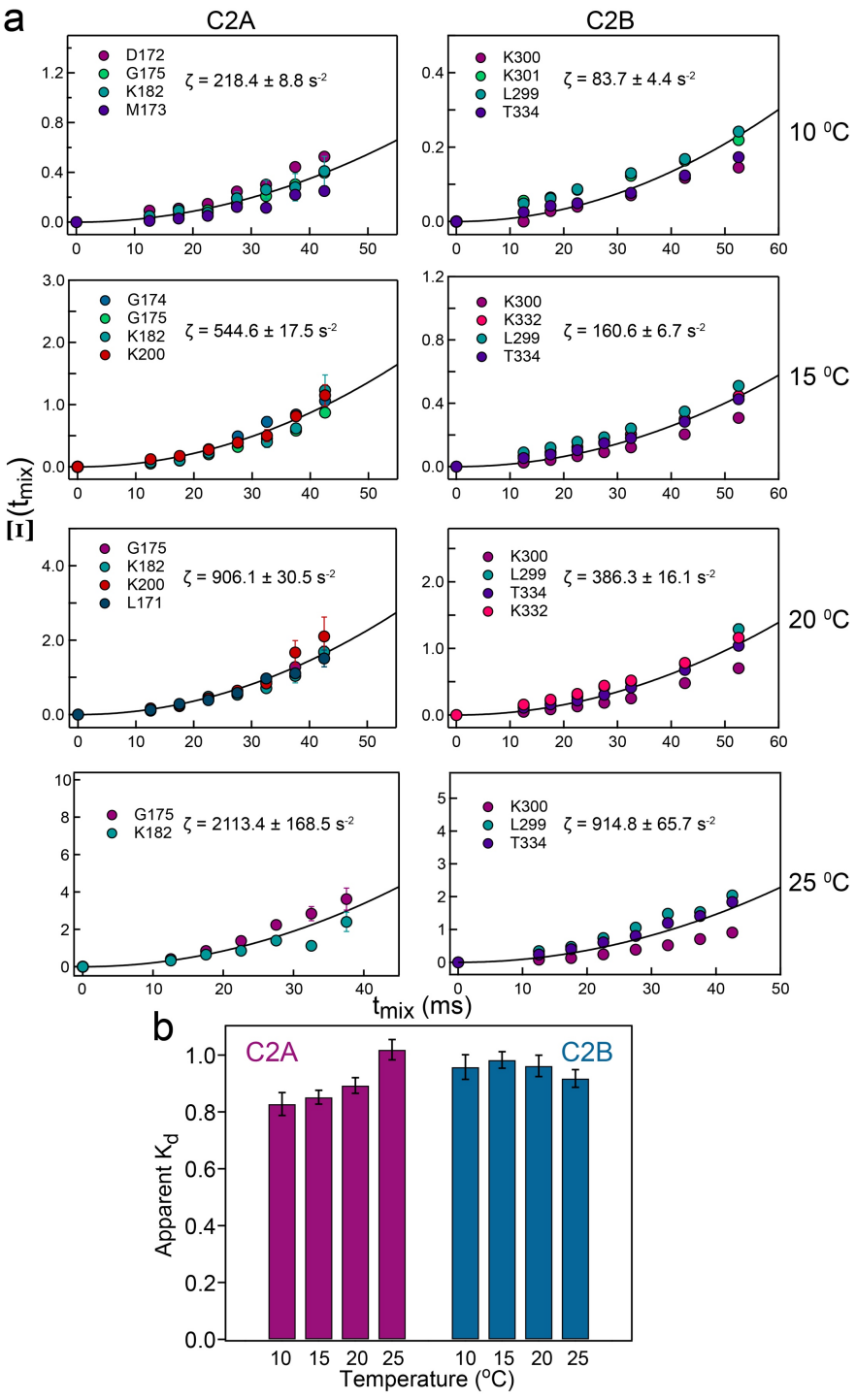

Figure S4. Analysis of the ZZ-exchange NMR data for the C2A and C2B domains. (**a**) Mixing time dependence of the composite peak intensity ratios Ξ, for which the auto- and cross-peaks have high S/N ratios and are well-resolved. Solid lines represent the fits to **Eq. S1**. (**b**) The average apparent K_d values (Eq. 6) determined using fully relaxed ^{15}N-^{1}H HSQC data, collected with the recycle delay of 6 s. The error bars represent the standard deviations of 8 (C2A) and 12 (C2B) residues.

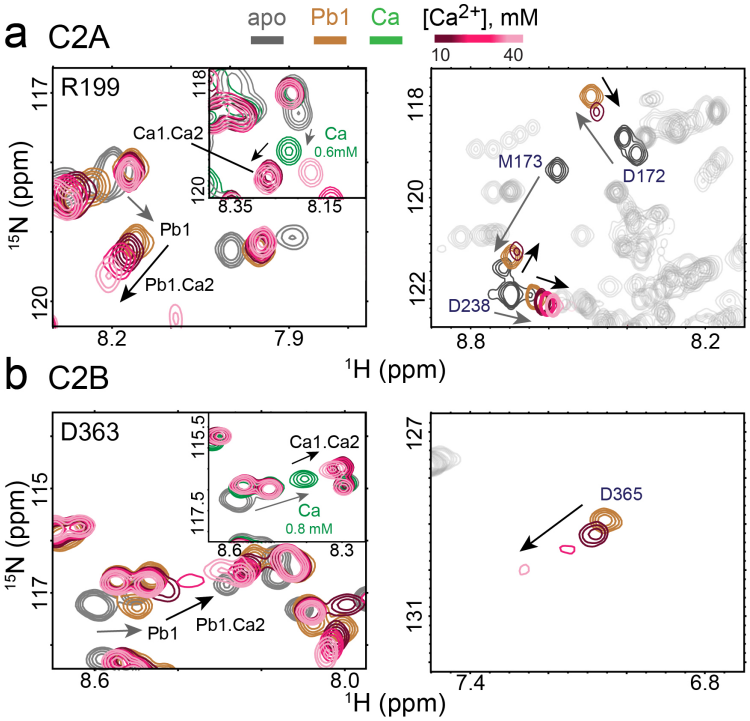

Figure S5. Expansions of the ^{15}N-^{1}H HSQC spectra showing Ca^{2+}-binding behavior of Arg199, Met173, Asp172, and Asp238 in C2A·Pb1 (**a**) and Asp363 and Asp365 in C2B·Pb1 (**b**). The C2 states are: apo (gray), C2·Pb1 (sienna), and C2·Ca1/Ca2 (green), the latter representing C2 domains at intermediate Ca^{2+} concentrations. The insets show cross-peak trajectories obtained in Ca^{2+}-only binding experiments. While not even 40 mM Ca^{2+} is sufficient to saturate Site 2 of C2·Pb1 complexes, Site 2 saturates at <10 mM Ca^{2+} in the absence of pre-bound Pb^{2+}.

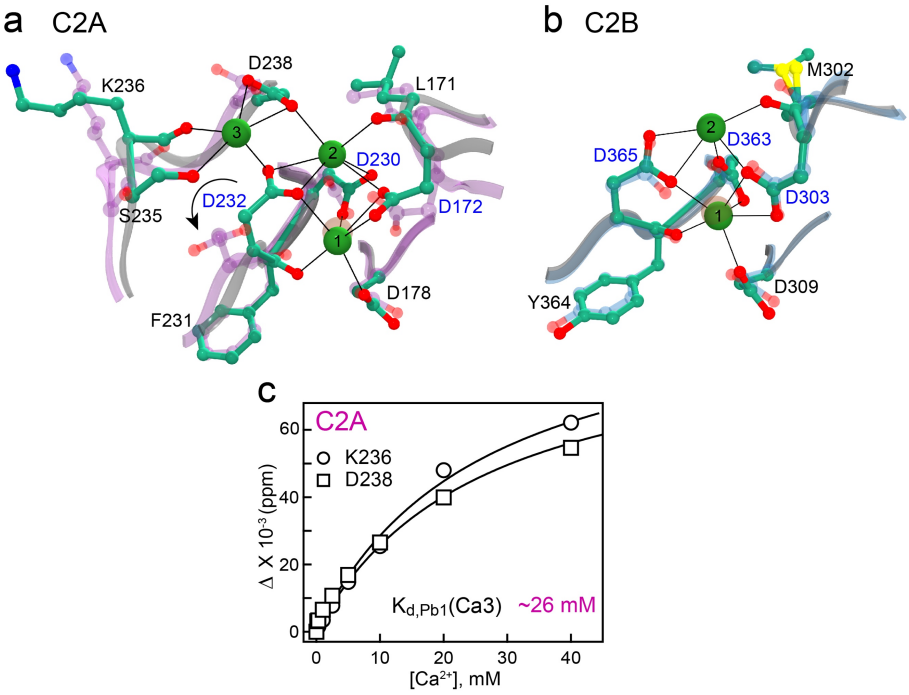

Figure S6. Population of Site 1 by Pb^{2+} affects Ca^{2+} binding to Site 2. (**a**) Overlay of the C2A loop regions in the Ca^{2+}-complexed C2A (1byn/NMR, green side chains) and the C2A·Pb1 complex (5vfe, purple side chains). (**b**) Overlay of the C2B loop regions in the Ca^{2+}-complexed C2B (1tjx, green side chains) and the C2B·Pb1 complex (5vfg, blue side chains). Asp sidechains that serve as bridging residues between metal ions occupying Sites 1 and 2 are shown in blue in (**a,b**). (**c**) Ca^{2+}-binding curve for Site 3 of the C2A·Pb1 complex. The estimated dissociation constant obtained from fitting the curves (solid lines) is 26 mM.

TABLES

Table S1. X-ray diffraction data collection and refinement statistics for the Pb^{2+} complexes of C2A and C2B.

	C2A·Pb (5vfe)	C2B·Pb, low occupancy (5vff)[a]	C2B·Pb, high occupancy (5vfg)
Data collection			
Space group	$P3_2$	$P2_12_12_1$	$P2_12_12_1$
Cell dimensions			
a, b, c (Å)	55.0, 55.0, 77.2	40.6, 41.1, 82.9	40.5, 41.3, 83.5
α, β, γ(°)	90, 90, 120	90, 90, 90	90, 90, 90
Wavelength (Å)	1.54178	1.54178	1.54178
Resolution (Å)	40.55 - 1.38 (1.45 - 1.38)[b]	41.43 - 1.41 (1.49 - 1.41)	41.28 - 1.82 (1.92 - 1.82)
R_{sym}	0.064 (0.619)	0.056 (0.617)	0.108 (0.532)
R_{pim}	0.022 (0.317)	0.023 (0.266)	0.073 (0.365)
Mean ($I/\sigma I$)	18.0 (2.2)	22.7 (2.9)	7.9 (2.0)
Completeness (%)	100 (99.8)	99.0 (95.9)	99.2 (99.3)
Redundancy	8.2 (4.6)	6.6 (6.0)	3.0 (3.0)
Wilson B-factor ($Å^2$)	13.6	12.1	15.7
Refinement			
Resolution (Å)	29.99 - 1.38	36.48 - 1.41	20.64 - 1.82
No. Unique Reflections	53,727	26,980	12,971
R_{work} / R_{free}	0.145/0.178	0.153/0.192	0.197/0.260
No. Atoms			
Protein	2,055	1,228	1,220
Ligand	12 (2 Pb^{2+}, 2 SO_4^{2-})	1 (Pb^{2+})	1 (Pb^{2+})
Solvent	355	251	229
B-factors ($Å^2$)			
Protein	21.1	15.6	19.4
Ligand	31.7	19.2	18.8
Solvent	32.8	28.6	26.6
R.m.s. deviations			
Bond lengths (Å)	0.007	0.006	0.007
Bond angles (°)	1.080	0.887	0.823
Ramachandran Plot			
Favored (%)	98.8	98.7	97.3
Allowed (%)	1.2	1.3	2.7
Outliers (%)	0.0	0.0	0.0

[a]The "low-occupancy" structure contains a single Pb^{2+} ions whose coordination sphere is incomplete.
[b]The numbers in parentheses correspond to the highest resolution bin.

Table S2. C2A r.m.s.d. values calculated for the backbone Cα carbons.

C2A (pdb ID)	*Apo (4wee)*	*Ca^{2+} (1byn)*	*Mn^{2+} (3f05)*	***Pb^{2+} Chain A (5vfe)***	***Pb^{2+} Chain B (5vfe)***
Apo (4wee)	0	1.12	0.38	1.20	1.08
Ca^{2+} (1byn)		0	0.91	1.23	0.95
Mn^{2+} (3f05)			0	1.03	0.92
Pb^{2+} Chain A (5vfe)				0	0.82
Pb^{2+} Chain B (5vfe)					0

Table S3. C2B r.m.s.d. values calculated for the backbone Cα carbons.

C2B (pdb ID)	*Apo (5ccj)*	*Ca^{2+} (1tjx)*	*Sr^{2+} (1tjm)*	***Pb^{2+} High Occupancy (5vfg)***	***Pb^{2+} Low Occupancy (5vff)***
Apo (5ccj)	0	0.65	0.71	0.68	0.88
Ca^{2+} (1tjx)		0	0.18	0.65	0.75
Sr^{2+} (1tjm)			0	0.67	0.77
***Pb^{2+} High Occupancy* (5vfg)**				0	0.30
***Pb^{2+} Low Occupancy* (5vff)**					0

Table S4. Metal-oxygen distances in the crystal structures of C2A of Syt1.

Ligand	*Cd^{2+} (5t0r)*	*Mn^{2+} (3f05)*	***Pb^{2+} chain A (5vfe)***	***Pb^{2+} chain B (5vfe)***
Asp172 Od1	2.92		2.52	2.55
Asp172 Od2	2.42	2.00	2.49	2.47
Asp178 Od2	2.40	2.31	2.90	2.74
Asp230 Od1	2.44	2.34	2.67	2.66
Asp230 Od2	2.61		2.53	2.59
Phe231 O	2.52	2.38	2.82	2.88
Asp232 Od2		2.16		
HOH	#403, 2.57	#81, 2.81	#525 2.74	#540, 2.81
HOH		#455, 3.63	#442 2.69	#466, 2.82
Average Distance	2.55	2.52	2.67	2.69
Total number of ligands	7 (6 protein, 1 water)	7 (5 protein, 2 waters)	**8 (6 protein, 2 waters)**	**8 (6 protein, 2 waters)**

Table S5. Metal-oxygen distances in the crystal structures of C2B of Syt1.

Ligand	*1st Ca^{2+} (1tjx)*	*Cd^{2+} (5t0s)*	***Pb^{2+} High occupancy (5vfg)***	***Pb^{2+} Low occupancy (5vff)***
Met302 O				
Asp303 Od1	2.51	2.76	2.60	
Asp303 Od2	2.56	2.72	2.77	
Asp309 Od1	2.50			
Asp309 Od2		2.67	2.71	2.60
Asp363 Od1		2.48	2.62	
Asp363 Od2	2.48	2.75	2.50	2.58
Tyr364 O	2.41	2.56	2.64	2.78
Asp365 Od1	2.49		2.44	2.53
Asp365 Od2				
HOH	#109, 2.41	#203, 2.26	#189, 2.83	
HOH				#199, 2.29
HOH				#250, 2.92
Average Distance	2.48	2.60	2.64	2.62
Total number of ligands	7 (6 protein, 1 water)	7 (6 protein, 1 water)	**8 (7 protein, 1 water)**	**6 (4 protein, 2 waters)**

Table S6. Kinetic parameters of Pb^{2+} binding to Site 1 of C2 domains obtained from the analysis of the ZZ exchange NMR data.

Domain	*Kinetic Parameters*	*10 ^0C*	*15 ^0C*	*20 ^0C*
C2A	k_{on}' (s^{-1})	17.2 ± 0.5	25.3 ± 0.5	31.9 ± 0.7
	k_{on} ($M^{-1}s^{-1}$) x 10^7	2.7 ± 0.2	3.8 ± 0.1	4.6 ± 0.2
	k_{off} (s^{-1})	14.2 ± 0.8	21.5 ± 0.8	28.4 ± 1.1
	k_{ex} (s^{-1})	31.4 ± 1.0	46.8 ± 1.0	60.3 ± 1.3
C2B	k_{on}' (s^{-1})	9.3 ± 0.3	12.8 ± 0.3	20.0 ± 0.6
	k_{on} ($M^{-1}s^{-1}$) x 10^7	3.3 ± 0.2	3.8 ± 0.1	4.9 ± 0.2
	k_{off} (s^{-1})	8.6 ± 0.5	12.6 ± 0.5	19.3 ± 1.0
	k_{ex} (s^{-1})	18.3 ± 0.6	25.3 ± 0.6	39.3 ± 1.1

REFERENCES

1. S. Katti, S. B. Nyenhuis, B. Her, A. K. Srivastava, A. B. Taylor, P. J. Hart, D. S. Cafiso and T. I. Igumenova, Non-Native Metal Ion Reveals the Role of Electrostatics in Synaptotagmin 1-Membrane Interactions, *Biochemistry*, 2017, **56**, 3283-3295.
2. W. Kabsch, XDS, *Acta Crystallogr. Sect. D. Biol. Crystallogr.*, 2010, **66**, 125-132.
3. A. J. McCoy, R. W. Grosse-Kunstleve, P. D. Adams, M. D. Winn, L. C. Storoni and R. J. Read, Phaser crystallographic software, *J. Appl. Crystallogr.*, 2007, **40**, 658-674.
4. Y. Cheng, S. M. Sequeira, L. Malinina, V. Tereshko, T. H. Sollner and D. J. Patel, Crystallographic identification of Ca2+ and Sr2+ coordination sites in synaptotagmin I C2B domain, *Protein Sci.*, 2004, **13**, 2665-2672.
5. P. D. Adams, P. V. Afonine, G. Bunkóczi, V. B. Chen, I. W. Davis, N. Echols, J. J. Headd, L.-W. Hung, G. J. Kapral and R. W. Grosse-Kunstleve, PHENIX: a comprehensive Python-based system for macromolecular structure solution, *Acta Crystallogr. Sect. D. Biol. Crystallogr.*, 2010, **66**, 213-221.
6. P. Emsley, B. Lohkamp, W. G. Scott and K. Cowtan, Features and development of Coot, *Acta Crystallogr. Sect. D. Biol. Crystallogr.*, 2010, **66**, 486-501.
7. V. Z. Miloushev, F. Bahna, C. Ciatto, G. Ahlsen, B. Honig, L. Shapiro and A. G. Palmer III, Dynamic properties of a type II cadherin adhesive domain: implications for the mechanism of strand-swapping of classical cadherins, *Structure*, 2008, **16**, 1195-1205.